A multi-feature-based fault diagnosis method based on the weighted timeliness broad learning system

Wenkai Hu[a,b,c], Yan Wang[a,b,c], Yupeng Li[a,b,c,*], Xiongbo Wan[a,b,c], R. Bhushan Gopaluni[d]

[a]*School of Automation, China University of Geosciences, Wuhan 430074, China*
[b]*Hubei Key Laboratory of Advanced Control and Intelligent Automation for Complex Systems, Wuhan 430074, China*
[c]*Engineering Research Center of Intelligent Technology for Geo-Exploration, Ministry of Education, Wuhan 430074, China*
[d]*Department of Chemical and Biological Engineering, University of British Columbia, Vancouver, BC V6T 1Z3, Canada.*

Abstract

Accurate and timely fault diagnosis is a vital task to ensure process safety of modern industrial facilities. Motivated by the complex variations of process signals and mutual coupling of faults, this paper presents a multi-feature-based fault diagnosis method based on the weighted timeliness Broad Learning System (BLS). The proposed method fuses multiple features extracted from the original process data to improve the fault diagnosis performance, and makes the diagnosis model suitable for dynamic fault diagnosis problems by incorporating the BLS. The major contributions of this study are twofolds: 1) A systematic multi-feature extraction method is proposed to extract long-term trend features, short-term trend features, and binary alarm signals, which reflect the direction and amplitude changes of process signals under faulty conditions; 2) a weighted timeliness BLS structure with multiple fault-sensitive features as the input is proposed to ensure the dynamic characteristics of the fault diagnosis model. The designed fault diagnosis model can be updated in an incremental manner, and thus can improve the model updating efficiency while ensuring accuracy. The effectiveness and superiority of the proposed method is demonstrated by a case study based on the Tennessee Eastman benchmark process.

Keywords: Multi-feature fusion, broad learning system, qualitative trend analysis, alarm signal, fault diagnosis

1. Introduction

Safe and reliable process operations are of great importance to modern industrial facilities, such as oil refineries, chemical plants, metallurgical factories, and power utilities, as the presence of faults and plant failures may have widespread negative impact on the production, and even lead to huge economic losses and catastrophic consequences (Song et al., 2020; Bai and Zhao, 2023). Such industrial facilities are usually large-scale and include a number of interconnected equipment, vessels, and devices; due to the complexity in system dynamics, process connectivity, and production modes, it is a challenging task to achieve reliable process monitoring and accurate fault diagnosis (Liu et al., 2018). Especially, the traditional model based and statistical methods experience limitations in handling complex fault diagnosis problems. In the past decade, increasing attention has been given to data-driven approaches, especially artificial intelligence and big data technologies, with applications to fault detection and diagnosis (Men et al., 2023; Liu et al., 2022b). Such methods utilize fault-sensitive information in historical operational data to build diagnostic models and improve performance by optimizing model structure and parameters (Chen et al., 2021).

Classical multivariate statistical analysis methods have been widely used in fault detection. These methods investigate the relationships among variables by decomposing the multivariate space into statistical features that can reflect spatial variations, and then calculate the corresponding statistical indicators for process monitoring (Ji et al., 2017; Shang et al., 2018). Typical methods include Principal Component Analysis (PCA) (Cao et al., 2020), Independent Component Analysis (ICA) (Uddin et al., 2021), and Partial Least Squares (PLS) (Amin et al., 2021). A number of variants have been proposed to address the nonlinear characteristics, such as recursive least square (Lu et al., 2020), solified-PLS (Li et al., 2021a), and improved PLS related to key performance indicators (Yin et al., 2015). The main advantage of the above methods lies in little requirement for prior knowledge, while they may fall short of accurately identifying fault types.

Recently, various hybrid approaches of fault detection and diagnosis were proposed and integrated with risk assessment (Liu et al., 2023; Li et al., 2023a). Fault diagnosis is a task to diagnose the fault types in a system and essentially a multi-classification problem, while risk assess-

*Corresponding author
Email addresses: wenkaihu@cug.edu.cn (Wenkai Hu), cugwangyan1@163.com (Yan Wang), yupengli@cug.edu.cn (Yupeng Li), xbwan23@cug.edu.cn (Xiongbo Wan), bhushan.gopaluni@ubc.ca (R. Bhushan Gopaluni)

ment is a process for evaluating potential risks in a system, involving the identification, analysis, and mitigation of hazards (Cai et al., 2020, 2021; Kong et al., 2022). Risk assessment can enhance fault diagnosis by prioritizing the faults that pose higher risks to the system and help with determination of fault degrees based on the thresholds in risk assessment. It can also support continuous improvements of fault diagnosis models based on results gained through risk assessments and thus ensure that the diagnostic system remains effective over time. A system risk analysis method was proposed based on Bayesian networks (Zhang et al., 2018). Cheng et al. (2021) proposed a novel process monitoring framework based on canonical correlation analysis and matter-element model. By integrating gradient-boosted decision trees and a computational model, a hybrid approach was proposed for the early detection of hazardous system deviations (Vairo et al., 2023). Regarding the risk investigation, a dynamic risk modeling method was proposed based on Stochastic Petri net to analyze the urban natural gas pipeline accidents (Li et al., 2023b). The hybrid approach provides a novel path to ensure process safety and reduce the risk of accidents. However, the above methods are designed for specific risks and fall short in diagnosing multiple faults.

Faults are often accompanied by abnormal changes in process signals. Hence, extracting characteristics of abnormal changes is a key step in fault diagnosis. For instance, Song and He (2023) proposed a fault detection method based on residual signal computed based on reconstruction errors. Li et al. (2023c) exploited qualitative trend analysis to qualitatively describe the change direction of fault-related signals. Chen and Zhao (2021) established a hierarchical fault diagnostic model to cope with strong nonlinear characteristics. Li et al. (2021b) utilized multi-scale symbolic diversity entropy to quantify the dynamic complexity of signals. In (Liu et al., 2022a), a dynamic latent variable prediction method was proposed to capture dynamic relations between time-series. In addition to process signals, the benefits of alarm logs and alarm settings for fault diagnosis were demonstrated in Lucke et al. (2020a). Low and high alarm thresholds were defined according to the alarm position (Lucke et al., 2020b). A quantitative representation method for alarms was proposed based on the quantity and time-series distribution (Zhang et al., 2023). As a single feature can only reflect partial information from a certain perspective, multi-feature has been considered in the design of fault diagnosis methods. For instance, multi-scale features were extracted based on expert knowledge to diagnose faults in Li et al. (2020). Such multi-feature-based diagnostic methods were designed for specific processes, and thus were difficult to be applied to other processes.

Based on the extracted fault-related features, machine learning and neural networks have been widely exploited in the construction of fault diagnosis models. Especially, deep learning approaches have received extensive studies. Deep learning utilizes a large amount of data under various operating conditions to establish a mapping relationship between data and working conditions. In Xie et al. (2022), a novel intelligent diagnosis method was proposed based on Convolutional Neural Networks (CNN). An intelligent fault diagnosis method for rotating components was developed based on multi-feature and CNN (Arunthavanathan et al., 2021). An early fault detection method was proposed based on CNN-LSTM by examining the fault symptoms (Cheng et al., 2019). Although the above-mentioned CNN, RNN, and LSTM methods achieved good diagnosis performance, the complex model training and updating processes limited their industrial implementation.

In view of the extensive training and updating efforts of deep neural networks, an effective incremental learning system called Broad Learning System (BLS) was proposed (Chen and Liu, 2018). The BLS can be in an incremental way without relying on a deep network structure and exhibits excellent performance on multi-classification problems (Yu and Zhao, 2020; Gao et al., 2021). Benefiting from these distinct advantages, the BLS has been introduced to design data-driven fault diagnosis models. For instance, a single-layer feedforward network-based BLS was proposed for the rotating machinery fault diagnosis (Yang et al., 2023). Considering the difficulty of obtaining all faulty data at once, an improved BLS was proposed to develop a lifelong learning fault diagnosis model (Fu et al., 2023). Further, the sequential order of training data was integrated to develop an online semi-supervised BLS structure for fault diagnosis (Pu and Li, 2021). Even though much effort to deal with model architecture and update mechanisms has been made to provide reliable diagnosis results, current BLS structures fall short in handling the multiple features associated with industrial faults.

The above studies provide comprehensive and effective solutions for fault diagnosis based on multivariate statistical analysis and neural networks. However, there still exist many unsolved open problems. Especially, there are two critical limitations: 1) Most existing fault diagnosis methods rely on extensive continuous-valued process data or single types of features, making the fault-related characteristics not fully used and thus compromising the fault diagnosis performance. Thus, how to extract and fuse multiple features in the training of fault diagnosis model is the first problem to be investigated in this work. 2) Many deep learning based fault diagnosis models are complex in structure and computationally burdensome in model training, and they are also difficult to get updated with the presence of new unknown faults. By contrast, the BLS based models can overcome such limitations. How to handle the time dependencies of process signals and corresponding features in the model training and updating is another problem to be addressed in this work.

Motivated by the above discussions, this paper proposes a multi-feature-based fault diagnosis method based on the weighted timeliness Broad Learning System (BLS). The proposed method fuses multiple features extracted from the original process data to improve the fault diagno-

sis performance, and makes the diagnosis model suitable for dynamic fault diagnosis problems by incorporating the BLS. The major contributions of this work are as follows:

- A systematic multi-feature extraction method is proposed to extract long-term trend features, short-term trend features, and binary alarm signals, which reflect the direction and amplitude changes of process signals under faulty conditions.
- A weighted timeliness BLS structure with multiple features as the input is proposed to ensure the dynamic characteristics of the fault diagnosis model.

To demonstrate the effectiveness and superiority of the proposed method, a case study based on Tennessee Eastman benchmark process is presented and comparisons with other state-of-the-art methods are given.

The remainder of this paper is structured as follows: Section 2 describes the fault diagnosis problem. Section 3 presents the framework and method for multi-feature extraction. In Section 4, the systematic method for fault diagnosis based on the broad learning system is proposed. The effectiveness of the proposed method is demonstrated by a case study in Section 5, followed by conclusions in the final section.

2. Problem Description

In complex industrial processes, the transition from normal state to a faulty state is usually accompanied by significant changes in the amplitudes or trends of process signals (Wu and Zhao, 2018). Capturing these changes can facilitate the acquisition of fault-related information and thus is beneficial for accurate fault diagnosis. Typical changes in process signals are various, such as sudden increases over the threshold, slow decline over a period of time, and alternating upward and downward trends.

For instance, Fig. 1 shows the time series plots of two process variables, namely, E feed and stripper pressure of the benchmark Tennessee Eastman (TE) process (Ricker, 1996) under different states. The blue curve in $t \in [0, 500]$ corresponds to the normal state; the red and orange curves in $t \in [501, 980]$ denote the signals under faults 1 and 2, respectively. It can be observed from Fig. 1(a) that the E feed signal in the presence of fault 1 increased slightly and then decreased drastically, followed by oscillating changes. In Fig. 1(b), fault 1 made the stripper pressure increase sharply first and then decrease, followed by damped oscillations. Table 1 summarizes the trend changes of process signals under faulty states in a time window highlighted by the green rectangle in Fig. 1, where $\nearrow$ denotes the increasing trend and $\searrow$ indicates the decreasing trend. Besides, the table also presents the short-term trends of the two process variables under different faulty conditions; the stripper pressure exhibits slow fluctuations while high fluctuations can be observed in other scenarios.

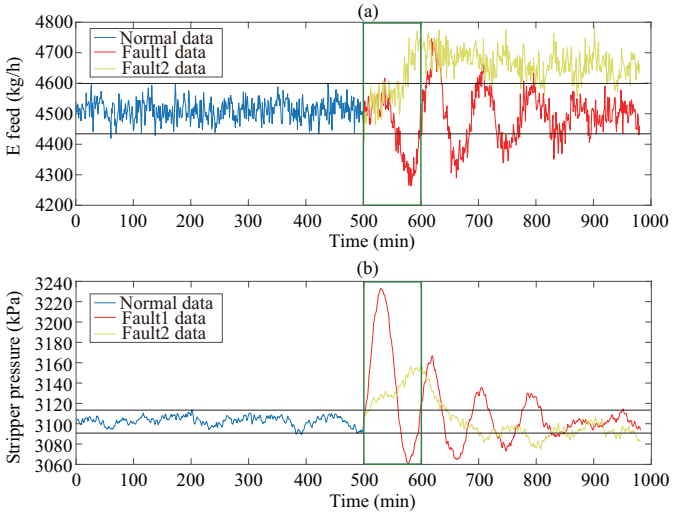

Figure 1: Time series plots of (a) the E feed and (b) the stripper pressure under different states of the Tennessee Eastman process.

Table 1: Trend changes of process variables under faults 1 and 2, respectively

Variable	Fault type	Long-term trend	Short-term trend
E feed	fault 1	$\nearrow\ \nearrow\ \nearrow$	High fluctuations
	fault 2	$\searrow\ \searrow\ \searrow$	High fluctuations
Stripper pressure	fault 1	$\nearrow\ \searrow\ \nearrow$	Low fluctuations
	fault 2	$\searrow\ \searrow\ \searrow$	High fluctuations

Long-term and short-term trends reflect the variational directions of process signals. In addition to that, the amplitude changes of process signals can be represented by alarm signals, which are obtained by comparing the process signals with the corresponding alarm thresholds. In Fig. 1, there are two black lines denoting the upper and lower thresholds of the process signals in the normal state, respectively. It can be found that the time series denoted by orange and red curves exceeded the normal ranges represented by the black lines under the two different faults. Hereby, alarm signals were generated to denote whether process signals exceed the normal operating ranges. As alarm signals are directly associated with faults, they can also key information to achieve accurate fault diagnosis.

This study aims to design a multi-feature-based fault diagnosis method for complex industrial processes to determine the type of faults accurately and promptly. As analyzed above, the key issues are to capture abnormal signal amplitude and trend changes under faulty conditions and fully using these features to build a diagnosis model. In this work, a multi-feature extraction method is designed to extract long-term and short-term trend features from process signals, as well as the corresponding alarm signals. Then, a weighted timeliness BLS structure is developed to process multi-features and train a fault di-

agnosis model. Moreover, a dynamic strategy to update fault diagnosis model parameters is designed to improve the adaptability of the method, so as to achieve good diagnostic performance.

3. Multi-Feature Extraction

This section presents the multi-feature extraction method to obtain trend features in different time scales and binary-valued alarm signals, which are key features imported by the BLS model.

3.1. Data De-Noising and Normalization

Process data collected in real industrial systems is usually contaminated by noises. To distill the trend features and alarm signals that are highly associated with faults, a foremost step is to improve the data quality. Here, an original signal $x(t)$ is represented by

$$x(t) = s\,(t) + \rho e\,(t)\,, t = 1, 2, \ldots, N \tag{1}$$

where $s\,(t)$ is the real signal, $e\,(t)$ denotes the Gaussian noise, ρ indicates noise level factor, t represents the time instant, and N is the number of samples. Considering that at the occurrence of a fault, process signals may exhibit obvious non-statioanry changes, the wavelet analysis as a commonly used data de-noising method applicable to non-stationary signals is exploited here to reduce noises and smooth the data (Pan et al., 1999). Denote the original time series as $x(1:N) = [x(1), x(2), \ldots, x(N)]$, and then the de-noised time series is represented by $\tilde{x}(1:N) = [\tilde{x}(1), \tilde{x}(2), \ldots, \tilde{x}(N)]$.

To avoid influence of amplitude ranges of process signals on feature extraction, the time series should be normalized into the same scale. Here, the min-max normalization is used. Given the de-noised signal $\tilde{x}(t)$, the normalized signal is obtained as

$$x_1(t) = \frac{\tilde{x}(t) - \min(\tilde{x})}{\max(\tilde{x}) - \min(\tilde{x})}, \tag{2}$$

where $\max(\tilde{x})$ and $\min(\tilde{x})$ are the maximum and minimum values of $\tilde{x}(1:N)$, respectively. Then, the de-noised and normalized time series is obtained as $x_1(1:N) = [x_1(1), x_1(2), \ldots, x_1(N)]$. For multiple process variables, the data matrix is denoted as X_1 of dimension $N \times M$, where N and M denote the numbers of samples and variables, respectively.

3.2. Short-Term Trend Extraction

In the presence of faults, some process signals, such as flow rates, may exhibit fast variations in high frequencies. Thus, it is common to extract short-term variational trends. In the short time scale, a sequence of short-term variational trends can be extracted based on the qualitative trend analysis. Given a preprocessed time series $x_1(1:N)$ showing short-term trends, the trend features are taken from one-step differences in a sliding window. The mean values of the previous period $\overline{x}_1(t-\tau)$ and the next period $\overline{x}_1(t+\tau)$ are calculated as (Li et al., 2020)

$$\overline{x}_1(t-\tau) = \frac{\sum_{i=1}^{\tau} x_1(t-i)}{\tau}, \tag{3}$$

$$\overline{x}_1(t+\tau) = \frac{\sum_{i=1}^{\tau} x_1(t+i)}{\tau}, \tag{4}$$

where τ represents the window length, which is set as several sampling cycles, and t denotes the time instant. Then, the differences between the mean values of two adjacent windows are calculated in two ways as

$$\triangle x_f\,(t) = x_1\,(t) - \overline{x}_1(t-\tau), \tag{5}$$

$$\triangle x_b\,(t) = \overline{x}_1(t+\tau) - x_1\,(t)\,, \tag{6}$$

where $\triangle x_f\,(t)$ and $\triangle x_b\,(t)$ represent the forward and backward one-step differences, respectively.

Then, the short-term trends $\triangle x_f\,(t)$ and $\triangle x_b\,(t)$ are defined as three states, namely, decreasing (-), unchanged (0), and increasing (+), i.e.,

$$s_f\,(t) = \begin{cases} -, & \triangle\, x_f\,(t) < -\lambda, \\ 0, & -\lambda \le \triangle x_f\,(t) \le \lambda, \\ +, & \triangle\, x_f\,(t) > \lambda, \end{cases} \tag{7}$$

$$s_b\,(t) = \begin{cases} -, & \triangle\, x_b\,(t) < -\lambda, \\ 0, & -\lambda \le \triangle x_b\,(t) \le \lambda, \\ +, & \triangle\, x_b\,(t) > \lambda, \end{cases} \tag{8}$$

where λ is a user-defined threshold; ideally, λ should be smaller than 1 and close to 0, so as to treat nonsignificant changes as the unchanged trend.

According to the short-term trends $\triangle x_f\,(t)$ and $\triangle x_b\,(t)$, a short-term qualitative state $s_q(t)$ is defined by two symbols in Fig. 2, namely, (-,-), (-,0), (-,+), (0,-), (0,0), (0,+), (+,-), (+,0), (+,+). Further, a short-term trend $s\,(t)$ is defined as

$$s\,(t) = \begin{cases} \text{H}, & s_q(t) = \text{VII or VI}, \\ \text{M}, & s_q(t) = \text{IV or IX}, \\ \text{L}, & s_q(t) = \text{I or III or V or VIII}, \\ \text{Z}, & s_q(t) = \text{II}, \end{cases} \tag{9}$$

where H, M, L, and Z represent high-fluctuation, medium-fluctuation, low-fluctuation, and non-fluctuation, respectively.

Given N samples corresponding to M_S variables with short-term trends, the corresponding short-term trend matrix is denoted by X_S, i.e.,

$$X_S = [s^1(1:N)^T, s^2(1:N)^T, \cdots, s^{M_s}(1:N)^T]_{N \times M_S}, \tag{10}$$

It should be noted that $M_S \le M$, since not all process variables have corresponding short-term features.

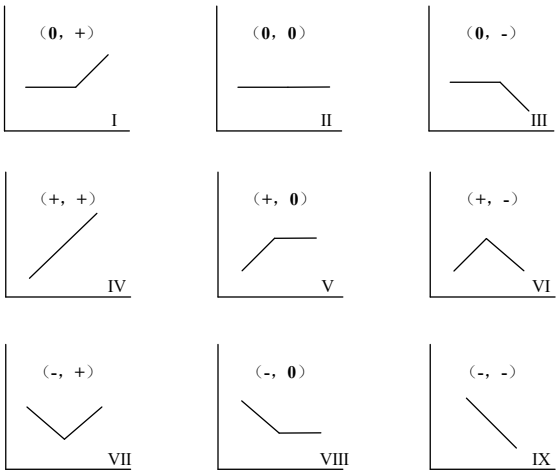

Figure 2: Definition of short-term trend signal.

3.3. Long-Term Trend Extraction

The short-term trend reflects volatility changes over a short period. However, some process signals, such as temperatures, may change slowly such that short-term trend extraction cannot capture their true variational trends. In this subsection, the long-time scale is considered in the extraction of trend features for slowly changing variables.

The time series is divided into several short lines by piece-wise linear representation (Wang et al., 2019; Hu et al., 2022). Suppose $x_1(1:N)$ is split into K segments connected end-to-end. The ith segment is represented by $x_1(t_i, t_{i+1}-1)$, where t_i and $t_{i+1}-1$ are the first and last sampling points, respectively. Each segment is assumed to be a linear regression model expressed as

$$y(t) = \hat{a}_i + \hat{k}_i t, t \in \{t_i, t_i+1, \cdots, t_{i+1}-1\}, \tag{11}$$

where $\hat{a}_i$ and $\hat{k}_i$ denote the estimated intercept and slope parameters of the ith segment, respectively. They can be obtained by the least square method (Abdi et al., 2007).

Then, the slope $k(t)$ corresponding to $x_1(t)$ is obtained by fitting the data of each segment. The long-term trend is defined as

$$l\left(t\right) = \begin{cases} 2, & k(t) \geq 1, \\ 1, & \varsigma < k(t) < 1, \\ 0, & -\varsigma < k(t) < \varsigma, \\ -1, & -1 < k(t) < -\varsigma, \\ -2, & k(t) \leq -1. \end{cases} \tag{12}$$

where 2, 1, 0, -1, and -2 represent fast-increasing, slow-increasing, unchanged state, slow-decreasing, and fast-decreasing, respectively; $\varsigma \in (0,1)$ is a threshold determined through experience.

In the above segmentation, it is necessary to determine the number of segments K, namely, how many segments a time series should be divided into (Wang et al., 2019). Given a group of samples $y(t_i : t_{i+1}-1)$ in the time period $[t_i, t_{i+1}-1]$, the convex hull composed by these samples is formed as A_i. Then, an index η_i representing the percentage of overlapped area in B_i is given by

$$\eta_i = \frac{|A_i \cap B_i|}{|A_i|}, \tag{13}$$

where the symbol $|\cdot|$ denotes the area of a 2-dimensional operand space. An index function $\eta(K)$ is defined as the weighted average of the indices $\eta_1, \eta_2, \cdots, \eta_K$, i.e.,

$$\eta(K) = \sum_{i=1}^{K} \frac{t_{i+1} - t_i}{N} \eta_i, \tag{14}$$

where $(t_{i+1} - t_i)$ is equal to the number of data points in the ith segment. The number of segments is eventually obtained as

$$\widehat{K} = \arg \max_{K} \eta(K). \tag{15}$$

In this way, the confidence interval includes as many data points as possible while minimizing the fitting error.

For variables with long-term trend features, the corresponding long-term trend matrix is denoted by X_L, i.e.,

$$X_L = [l^1(1:N)^T, l^2(1:N)^T, \cdots, l^{M_L}(1:N)^T]_{N \times M_L}, \tag{16}$$

where M_L represents the number of long-term feature variables and satisfies $M_L \leq M$.

3.4. Alarm Sequence Extraction

Either long-term trends or short-term trends only present the variational directions of process signals in the presence of a fault. Thus, it should extract features reflecting the change amplitudes of process signals. In modern industrial facilities, alarm limits are commonly configured, such that alarm events are generated to notify plant operators whenever the corresponding process signal exceeds its alarm limit. Compared to the original process signals and the trend features, alarms are directly associated with faults. Thus, it is natural to extract alarms from the original data and use it in fault diagnosis.

For each process variable, higher and lower alarm limits are configured. Given a signal conforming to the Gaussian distribution, its alarm limits can be simply calculated based on the historical data using the 3-sigma rule. For non-Gaussian distributed process data, kernel density estimation can be used to calculate the alarm limits (Węglarczyk, 2018). Then, the binary-valued alarm signal $x_a(t)$ is obtained by comparing the process signal with the alarm limits, i.e.,

$$a\left(t\right) = \begin{cases} 0, & T_L \leq x_1\left(t\right) \leq T_H, \\ 1, & \text{otherwise.} \end{cases} \tag{17}$$

where T_H and T_L denote the higher and lower alarm limits, respectively.

Similar to the long-term and short-term trend features,

X_A denotes the obtained alarm matrix, which is given by

$$X_A = [a^1(1:N)^T, a^2(1:N)^T, \cdots, a^{M_A}(1:N)^T]_{N\times M_A}, \tag{18}$$

where M_A represents the number of alarm variables and satisfies $M_A \leq M$.

3.5. Window Length Determination Based on Weighted Time-Cumulative Distribution

For online fault diagnosis applications, the three types features are extracted from the process signals in a sliding window. Here, the window length is an important parameter for online feature extraction. As the length of the sliding window increases, the trend feature information contained in the window become more abundant, but the computational time also increase. Thus, it is necessary to balance the accuracy and time consumption by determining an optimal value P_{wl} for the window length.

After piecewise linearization during the off-line feature extraction, the cumulative distribution probability P_c varying with online window length L is obtained, i.e.,

$$P_c(L) = P(l \leq L) \tag{19}$$

where $L \in [1, 2, \cdots, L_{max}]$, and L_{max} denotes the maximum window length of the long-term trend. The probability P_c increases as the window length increases, but it also prolongs the online feature extraction time. To balance the accuracy and time delay, a weighted time-cumulative distribution W_{tp} index is defined for the window length L as follows

$$W_{tp}(L) = \alpha_{tp} P_c(L) - (1-\alpha_{tp})\,\Delta t(L) \tag{20}$$

$$\Delta t(L) = \frac{t(L-1) - t(L)}{t(L-1)} \tag{21}$$

where α_{tp} indicates the window length weight factor. Here, the range of α_{tp} is [0,1]. The closer α_{tp} is to 1, the more important accuracy is in the fault diagnosis model. Conversely, the computational time is prioritized. On balance, α_{tp} is chosen as 0.5. Then, the optimal window length P_{wl} is estimated by maximizing W_{tp} as

$$P_{wl} = \arg \max_{L\in[1,L_{max}]} W_{tp}(L). \tag{22}$$

4. Broad Learning System Based Fault Diagnosis with Weighted Timeliness

This section presents the proposed dynamic fault diagnosis method based on the weighted timeliness Broad Learning System (BLS). Fig. 3 shows the flowchart of the method. There are three major steps: First, a feature combinator is designed to combine multiple features, which are extracted using the approaches in Section 3. Then, BLS-based fault diagnosis subsystems are developed by incorporating multiple weighted parameters based on multiple features, so as to improve the online model updating performance. Last, a decision-weighted fusion level is constructed to obtain the final fault diagnosis result by incorporating the outputs from multiple subsystems.

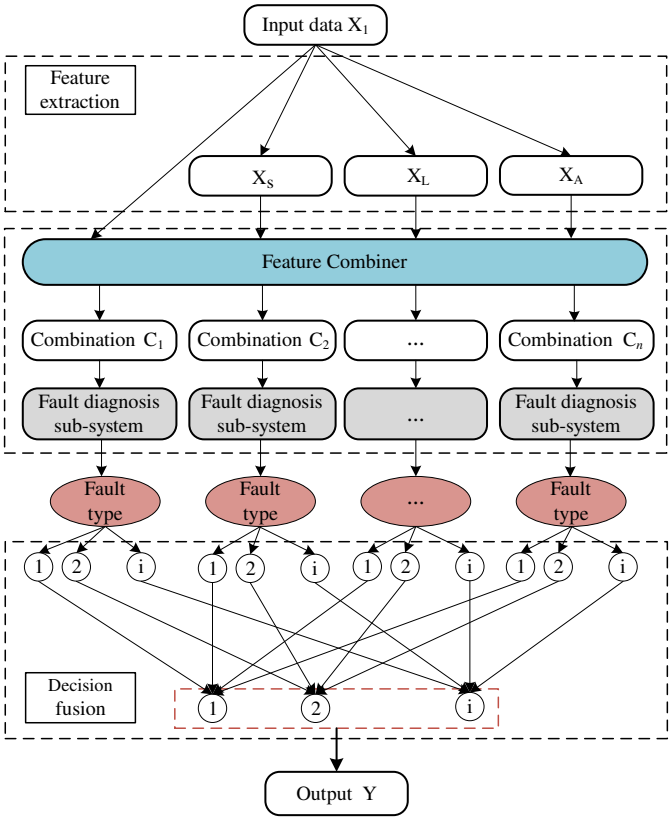

Figure 3: The flowchart of the fault diagnosis with weighted timeliness Broad Learning System.

4.1. Feature Combiner Based on Weighted Time-Accurate Fault Diagnosis Subsystem

Considering that multiple features contain different fault-related information, this subsection aims to design a fault diagnosis sub-system incorporating multiple features while ensuring the online diagnosis performance. First, the three feature matrices X_A, X_S, and X_L and the original matrix X_1 are fed into the feature combiner to obtain the feature combination. Table 2 shows the 15 combinations of the 4 types of features. Then, multiple combinations are input to the fault diagnosis sub-systems to compare the performance of the different initial combinations.

Fig. 4 shows the structure of a fault sub-system module. In each fault sub-system module, the fault diagnosis performance is improved by multi-layer BLS overlay; and the weighted time parameter is designed to ensure the dynamics of fast update of the model in online fault diagnosis. The sub-system structure with n sub-system BLS blocks $u_1, u_2, \cdots, u_n$ is described below.

Given the feature combination $\mathbf{C} \in \mathbb{R}^{N_c \times M_c}$ as the input, the associated labels $\mathbf{y} \in \mathbb{R}^{N_c \times 1}$ is the output label, where N_c and M_c indicate the number of samples and

Table 2: List of multi-feature tag, which corresponds to different combinations of features.

Tag	Feature	Tag	Feature	Tag	Feature
C_1	X_1	C_6	X_1, X_S	C_{11}	X_1, X_A, X_S
C_2	X_S	C_7	X_1, X_L	C_{12}	X_1, X_S, X_L
C_3	X_L	C_8	X_A, X_S	C_{13}	X_1, X_A, X_L
C_4	X_A	C_9	X_A, X_L	C_{14}	X_A, X_S, X_L
C_5	X_1, X_A	C_{10}	X_S, X_L	C_{15}	X_1, X_A, X_S, X_L

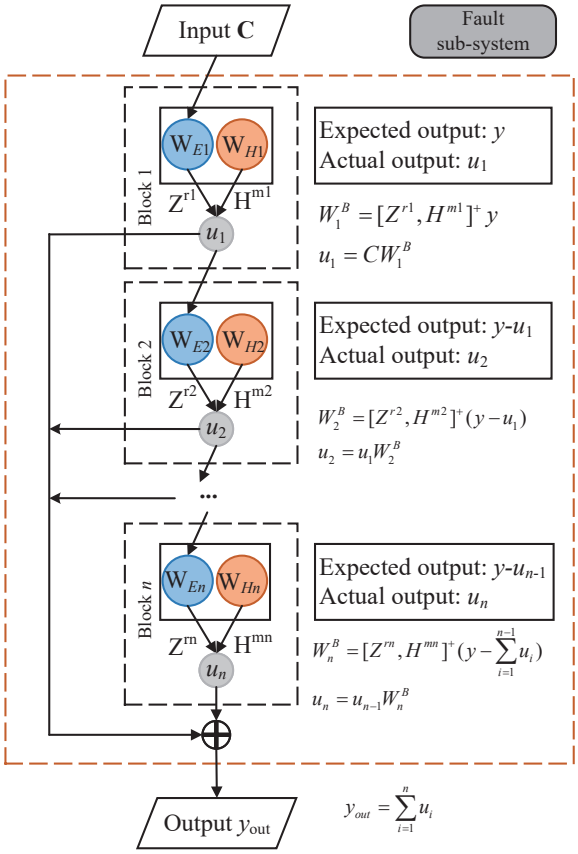

Figure 4: The flowchart of fault diagnosis subsystem of BLS with n-layer structure.

features, respectively. Assuming that the network is constructed by r feature mapping with m nodes per set, the ith group of mapped features $\mathbf{Z}_i$ is

$$\mathbf{Z}_i = \Phi(\mathbf{C}\mathbf{W}_{Ei} + \beta_{Ei}), i = 1, 2, \ldots, r \tag{23}$$

where $\mathbf{W}_{Ei}$ and β_i are the weights and offsets that are randomly generated; $\Phi(\cdot)$ is a linear activation function.

Denote the concatenation of all the r groups of mapped features as $\mathbf{Z}^r = [\mathbf{Z}_1, \mathbf{Z}_2, \ldots \mathbf{Z}_r]$. Then, the mth group of enhancement nodes is

$$\mathbf{H}_m = \zeta(\mathbf{Z}^r\mathbf{W}_{Hm} + \beta_{Hm}), \tag{24}$$

where $\mathbf{W}_{Hm}$ and β_{Hm} are the weights and bias that are randomly generated; $\zeta(\cdot)$ is a tanh activation function.

The concatenation of all the first m groups of enhancement nodes are denoted as $\mathbf{H}^m = [\mathbf{H}_1, \mathbf{H}_2, \ldots \mathbf{H}_m]$. The input matrix $\mathbf{A} = [\mathbf{Z}^r | \mathbf{H}^m]$ is composed of $\mathbf{Z}^r$ and the enhancement node $\mathbf{H}^m$. Hence, the broad model is represented as

$$\begin{aligned} \mathbf{Y} &= \mathbf{A}\mathbf{W}_a^B \\ &= [\mathbf{Z}^r, \mathbf{H}^m]\mathbf{W}_a^B \\ &= [\mathbf{Z}_1, \mathbf{Z}_2, \ldots \mathbf{Z}_r, \mathbf{H}_1, \mathbf{H}_2, \ldots \mathbf{H}_m]\mathbf{W}_a^B \end{aligned} \tag{25}$$

where $\mathbf{W}_a^B = \mathbf{A}^+\mathbf{Y}$ denotes the ath connecting weights for the broad structure, and $\mathbf{A}^+$ is the pseudo inverse of $\mathbf{A}$ and calculated by ridge regression (Chen and Liu, 2018).

At the first level of the subsystem, on the basis of the connection weight $\mathbf{W}_1^B$, and the output $\mathbf{u}_1$ of the first BLS block is calculated as

$$\mathbf{u}_1 = \mathbf{C}\mathbf{W}_1^B, \tag{26}$$

where $\mathbf{C}$ denotes the input feature combination. Then, the residual difference between the actual output and the expected output $\mathbf{y}$ is calculated as

$$\mathbf{d}_1 = \mathbf{y} - \mathbf{u}_1. \tag{27}$$

The residual $\mathbf{d}_1$ is taken as the target output of the second layer. Extending from a single-layer structure to a multi-layer structure, the final residuals of an a-layer network can be defined as

$$\mathbf{d}_a = \mathbf{y} - \sum_{k=1}^{a} \mathbf{u}_k. \tag{28}$$

The time required for training a fault diagnosis subsystem with a layers is

$$\hat{t}_a^{\text{bls}} = \sum_{k=1}^{a} t_k^{\text{bls}} \tag{29}$$

where t_k^{bls} denotes the time to train the kth layer.

As the number of layers increases, the final residuals would decrease and better performance of the fault diagnosis subsystem can be achieved. However, the time consumption for offline training and online fault diagnosis increases exponentially. This makes it difficult to balance online fault diagnosis performance with model updating efficiency. Accordingly, a weighted time-accuracy evaluation index is proposed and defined as

$$W_{ta}(a) = \alpha_{ta} * \Delta\mathbf{d}(a) - (1 - \alpha_{ta}) * \Delta t_a^{\text{bls}} \tag{30}$$

$$\Delta\mathbf{d}(a) = \frac{1}{N_c}\sum_{i=1}^{N_c}\sqrt{(\left|\mathbf{d}_{a-1}^{(i)}\right| - \left|\mathbf{d}_a^{(i)}\right|)^2} \tag{31}$$

$$\Delta t_a^{\text{bls}} = \frac{t_a^{\text{bls}}}{\hat{t}_{a-1}^{\text{bls}}} = \frac{t_a^{\text{bls}}}{\sum_{k=1}^{a-1} t_k^{\text{bls}}} \tag{32}$$

where $\Delta\mathbf{d}(a)$ denotes the residual gain rate of the a-layer BLS block; Δt_a^{bls} represents the time consuming gain rate of the BLS block; α_{ta} indicates the weight factor.

If $W_{ta}(a) > 0$, it takes u_a as the input and $\mathbf{d}_a$ as the desired output of the $a+1$th BLS block, i.e.,

$$\mathbf{d}_a = \mathbf{u}_a \mathbf{W}_{a+1}^B \tag{33}$$

Otherwise, the BLS block is eliminated, the offline training phase is completed, and the total number of layers of the final BLS block is finalized. Eventually, the actual output $\mathbf{y}_{\text{out}}$ is approximated by the sum of all outputs of the n BLS blocks as

$$\mathbf{y}_{\text{out}} = \sum_{k=1}^{n} \mathbf{u}_k. \tag{34}$$

According to the above calculations, the training procedure of a fault diagnosis sub-system is summarized in Algorithm 1.

Algorithm 1 Training procedure of a fault diagnosis subsystem.

Input: Feature combination $\mathbf{C}$; target $\mathbf{y}$; parameter α_{ta}

Output: Parameter matrix $\mathbf{W}^B$;

$i \leftarrow 2$, $dv_0 = y$, $\mathbf{u}_1 = \mathbf{C}\mathbf{W}_1^B$, $W_{ta}(i) = 1$
while $W_{ta}(i) > 0$ **do**
  $i \leftarrow i + 1$
  $\mathbf{W}_i^B$ by $\mathbf{W}_a^B = \mathbf{A}^+\mathbf{Y}$
  $\mathbf{u}_i = \mathbf{u}_{i-1}\mathbf{W}_i^B$
  $\mathbf{d}_i = \mathbf{y} - \sum_{k=1}^{i} \mathbf{u}_k$
  $\Delta\mathbf{d}_i = |\mathbf{d}_{i-1}| - |\mathbf{d}_i|$
  $\Delta t_i^{\text{bls}} = \frac{t_i^{\text{bls}}}{\hat{t}_{i-1}^{\text{bls}}} = \frac{t_i^{\text{bls}}}{\sum_{k=1}^{i-1} t_k^{\text{bls}}}$
  $W_{ta}(i) = \alpha_{ta} * \Delta dv_i - (1 - \alpha_{ta}) * \Delta t_i^{\text{bls}}$
end while
$\mathbf{W}^B = (\mathbf{W}_1^B, \mathbf{W}_2^B, \ldots, \mathbf{W}_i^B)$
return $\mathbf{W}^B$;

To evaluate the comprehensive performance of the subsystem, the accuracy of the sub-system is calculated as

$$\text{Acc} = \frac{\text{find}(\mathbf{y}_{\text{out}} \mid \mathbf{y})}{N_c} \tag{35}$$

where the function find$(\cdot)$ obtains the number of two-column vectors that are identical in the same position. All feature combinations $C_1, C_2, \ldots, C_{15}$ are taken as the input for the training process, and the corresponding results of multiple sub-systems are calculated as $\text{Acc}_1, \text{Acc}_2, \ldots, \text{Acc}_{15}$. Here, a selection parameter ϖ is defined; if $\text{Acc}_i \geq \varpi, i \in [1, ..., 15]$, the subsystem can be taken for online fault diagnosis. To find the best combination of fault diagnosis subsystems, the fault diagnosis subsystems are added successively according to the accuracy from highest to lowest.

4.2. Decision Weighted Fusion for Fault Determination

Considering that the fault-related information is reflected by multiple features, a decision-weighted fusion approach is developed to determine the final fault diagnosis results. The results of multiple fault diagnosis subsystems are combined with the historical rule base obtained by the feature combiner, and weighted fusion is performed to obtain the final diagnosis results.

Suppose that there are m fault diagnosis subsystems and e fault types, and the result of each subsystem is $y_1, y_2, \ldots, y_m$. The one-hot coding representation of the classification labels of the ith subsystem $\mathbf{d}_i, i = 1, 2, \cdots, m$ is denoted by

$$\mathbf{d}_i = \left[0, \ldots, 0, 1, 0 \ldots, 0\right]_{e\times 1}^T \tag{36}$$

with the jth element given by

$$\mathbf{d}_i^j = \begin{cases} 1, & y_i = j \\ 0, & \text{otherwise.} \end{cases} \tag{37}$$

According to the performance evaluation results of each fault diagnosis subsystem in Section 4.1, the weights $w_1, w_2, \ldots, w_i$ of each model are assigned as

$$w_i = \frac{\text{Acc}_i}{\sum_{i=1}^{m} \text{Acc}_i}. \tag{38}$$

Then, the weighted average of the results is obtained as

$$D = \text{dmax}\left|(w_1 * \mathbf{d}_1) \oplus (w_2 * \mathbf{d}_2) \oplus \cdots \oplus (w_m * \mathbf{d}_m)\right| \tag{39}$$

where dmax$|\cdot|$ takes the category with the highest probability of the fusion classification result and converts it into a category label; $\oplus$ denotes the operation of multiplying values by column vectors.

4.3. Procedures and Discussions

The proposed dynamic fault diagnosis method consists of two calculation phases, namely the offline training and online testing. In the training phase, the main steps include offline feature extraction and dynamic fault diagnosis model training. The major procedures of the offline training are summarized as follows:

(1) Offline feature extraction: The preprocessed data X_1 and three features X_S, X_L, and X_A are prepared and labeled with normal or fault categories; the optimal sliding window length P_{wl} for online feature extraction is selected.

(2) Dynamic fault diagnosis model training: The model is trained to get multiple multi-layer weight parameters $W^B(1), W^B(2), \ldots, W^B(m)$ and corresponding weight parameters W_P of the fault diagnosis model of the corresponding combination.

In the online fault diagnosis stage, the main steps include online feature extraction and dynamic fault diagnosis model training, which are summarized as follows:

(1) Online feature extraction: The online pre-processed data X_1^{OL} are obtained and analyzed to extract multiple features (X_S^{OL}, X_L^{OL}, X_A^{OL}) within a sliding window of length P_{wl}.

(2) Online fault diagnosis: The data and features X_1^{OL}, X_S^{OL}, X_L^{OL}, X_A^{OL} are firstly imported to the fault diagnosis model to obtain multiple feature combination $C_1, C_2, \ldots, C_m$, which are then taken by the corresponding fault diagnosis subsystems to obtain m fault diagnosis classification results $Y_1, Y_2, \ldots, Y_m$, where $Y_i = C_i W^B(i), i = 1, 2, \ldots, m$. Then, $Y_1, Y_2, \ldots, Y_m$ are converted to the one-hot form $D = D_1, D_2, \ldots, D_m$, combined with the off-line weight parameter W_P to obtain the final fault diagnosis result D of decision weighted fusion by eqn. (39). When there is a new fault type, the fault diagnosis model can be quickly updated by incrementally learning the parameters in the fault diagnosis subsystem and BLS.

To evaluate the fault diagnosis performance, four metrics, namely, Accuracy, Macro-Precision, Macro-Recall and Macro-F1 are exploited. They are given by

$$\text{Accuracy} = \frac{N_{\text{TP}}}{N_{\text{All}}}. \tag{40}$$

$$\text{Macro-Precision} = \frac{N_{\text{TP}}}{N_{\text{TP}} + N_{\text{FP}}}, \tag{41}$$

$$\text{Macro-Recall} = \frac{N_{\text{TP}}}{N_{\text{TP}} + N_{\text{FN}}}, \tag{42}$$

$$\text{Macro-F1} = \frac{2 * \text{Precision} * \text{Recall}}{\text{Precision} + \text{Recall}}, \tag{43}$$

where the true-negative N_{TN} and true-positive N_{TP} represent the numbers of correctly classified observations, the false-negative N_{FN} and false-positive N_{FP} represent the numbers of misclassifications, and N_{All} denotes the total number of samples (Hoang and Kang, 2019).

Remark 1. This study is motivated by process signals showing different variation characteristics in faulty conditions. Compared with the existing work, the main highlight of the method is in the following aspects: 1) The proposed method extracts multiple features include long-term trend features, short-term trend features, and binary alarm signals, whereas most existing fault diagnosis methods rely on extensive continuous-valued process data or single types of features (Li et al., 2023c; Lucke et al., 2020b); 2) the proposed fault diagnosis model considers the time dependencies of process signals and corresponding features in the model training and updating phases, whereas many other models were designed only for process signals or features (Zhang et al., 2023); 3) a weighted timeliness BLS structure is devised to balance the timeliness and accuracy, whereas current BLS structures fall short in handling the multiple features associated with industrial faults and computationally burdensome in model training (Chen and Liu, 2018; Gao et al., 2021).

5. Case Study

This section evaluates the performance of the proposed fault diagnosis method based on the data generated by the benchmark Tennessee Eastman (TE) process. TE process is widely used to test various fault diagnosis algorithms by simulating industrial processes with dynamic characteristics (Ricker, 1996). It includes 12 manipulated variables, 22 measured variables, and 18 component measurement variables. In the TE model, 21 different faults (16 known and 5 unknown faults) and normal states are considered. The 21 faults are divided into groups based on process signal trend features, such as step change, random change, slow shift, and valve stickiness. The basic information of the faults are shown in Table 3. Simulated data is collected for the normal state and all 21 faults. The training dataset contains 500 normal state samples and 480 samples for each type of fault. For the test set, there are 960 samples for each state.

Table 3: Fault types of the TE process.

Label	Description	Types
1	A/C feed ratio	step change
2	component B	step change
3	feed D temperature	step change
4	RCW inlet temperature	step change
5	CCW inlet temperature	step change
6	feed A loss	step change
7	C header pressure loss	step change
8	feed A-C components	random variation
9	feed D temperature	random variation
10	feed C temperature	random variation
11	RCW inlet temperature	random variation
12	CCW inlet temperature	random variation
13	reaction kinetics	slow drift
14	RCW valve	sticking
15	CCW valve	sticking
16	unknown	unknown
17	unknown	unknown
18	unknown	unknown
19	unknown	unknown
20	unknown	unknown
21	unknown	constant

5.1. Multi-Feature Extraction

This section sets the default parameters of the model, completes the offline feature extraction, and selects the sliding window length P_{wl}. Table. 4 shows the model parameters selected in this case study.

Table 4: Parameter setting for the case study

Parameter	λ	ς	α_{tp}	α_{ta}	$\min(P_c)$	ϖ
Default set	0.03	0.01	0.50	0.80	0.95	0.70

Fig. 5(a) shows the distribution of optimal segment length for the long-term trend, where the red area represents the density histogram. Fig. 5(b) shows the cumulative probability function and time consumption corresponding to different window lengths. As the window length increased, the blue and orange curves rose. This indicates that the sliding window contained more information while the time consumption increased. As shown in Fig. 5(c), the blue curve denotes the relationship between the indicator W_{TP} and different window lengths. At the point (44, 0.6012) marked by the red circle, W_{TP} reached its peak, indicating that $l = 44$ corresponded to the best performance of the weighted time-cumulative distribution. Therefore, the off-line training optimal window length $P_{wl} = 44$ is selected for online feature extraction.

To illustrate the feature extraction, visualization results are shown below based on the time series of the Separator Water (SW) temperature under the normal state, fault 1, and fault 2. Fig. 6 gives the time series plots for the normalized SW temperature in the 3 states, where subfigures (a), (b), and (c) correspond to the normal state, fault 1, and fault 2, respectively. It can be found that the temporal dependence of the SW temperature signal differed significantly in the above states.

The short-term trend extraction result is shown in Fig. 7, where H, M, L, and Z denote high-fluctuation, medium-fluctuation, low-fluctuation, and non-fluctuation, respectively. In the normal state, H is the major short-term trend that occurs most frequently; in fault 1, L is the more frequent short-term trend; in fault 2, the SW temperature had more H and L short-term trends. To better visualize the relations between short-term trends and different operating states, Fig. 8 presents the results of the variation of the short-term trend features across all the different states. The short-time trends under fault 6 and fault 18 were mostly concentrated in the Z zone, which is quite different from the other faults. It visualizes the differences between short-term features in different states and demonstrates that short-term trend features can provide helpful information about faults.

Fig. 9 shows the long-term trend extraction results by providing the variance of the same variable in different operating states. The red lines represent the long-term trends corresponding to different operating states. In the normal state, the trend of the signal was concentrated at 0, and there was no significant trend change; In fault 1, the long-term trend oscillated between 0, 1, 2, and -2; in fault 2, the long-term trend changed from 0 to 1, indicating the signal increased slowly.

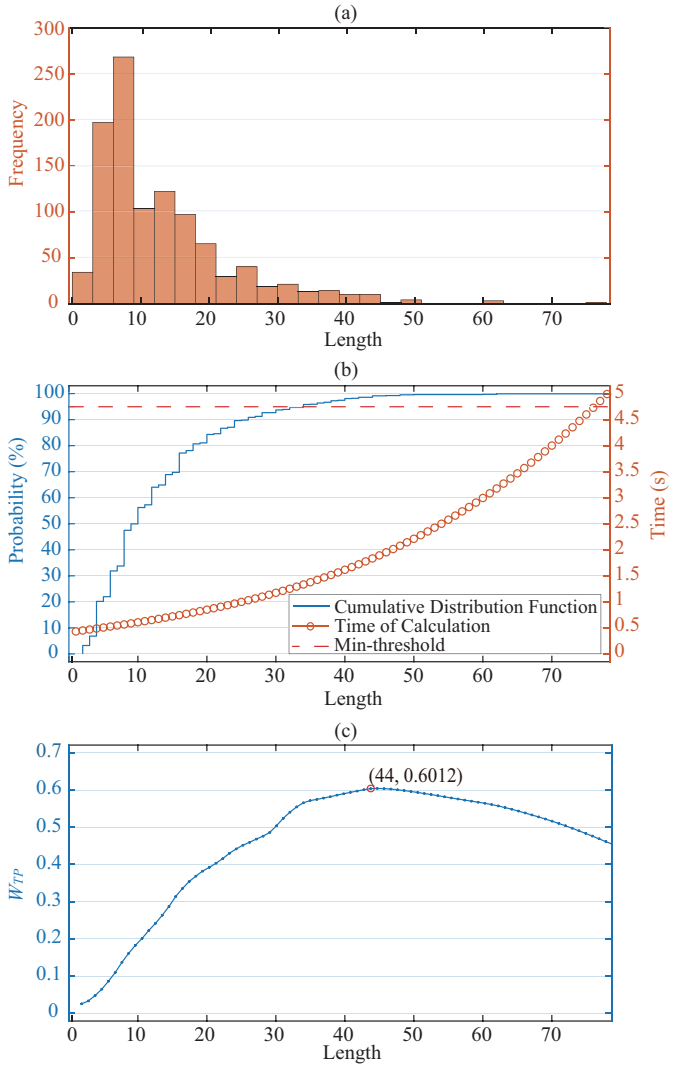

Figure 5: Sliding window length selection in online fault diagnosis, (a) Distribution of optimal segment length for long-term trend; (b) Cumulative probability function and time consumption corresponding to different window lengths; (c) Change curve of W_{TP} under different window lengths.

To evaluate the impact of the extracted multiple features on the fault diagnosis results, a comparative experiment was designed to demonstrate the effectiveness of Multi-Feature Extraction (MFE) for obtaining fault-related information. Other classical feature extraction methods, including PCA, Dynamic PCA (DPCA) (Dong and Qin, 2018), and Dynamic LDA (DLDA) (Yang and Gu, 2019), were adopted to extract features. Two classifiers were used, including the Support Vector Machine (SVM) and the Broad Learning System (BLS). Several faults, including faults 1, 2, 6, 7, and 8, were used in the test. Table 5 shows the fault diagnosis results of the two classifiers based on different feature extractors. It can be seen that in the two cases with SVM and BLS as the classifiers, highest accuracies were achieved when the proposed Multi-Feature Extraction method was applied. This demonstrates the superiority of the method in extracting fault-related fea-

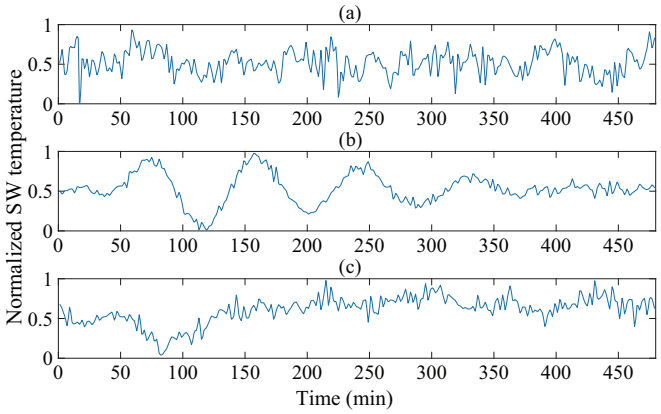

Figure 6: Time series of the separator water temperature under different states; (a) (b), and (c) correspond to the normal state, fault 1, and fault 2, respectively.

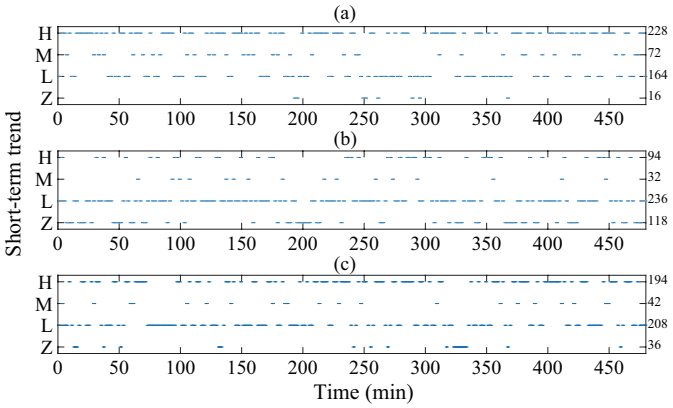

Figure 7: Short-term trends of the separator water temperature under (a) the normal state, (b) fault 1, and (c) fault 2, respectively.

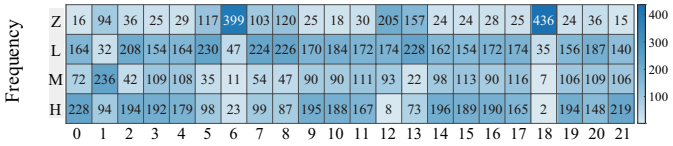

Figure 8: Statistical plot of short-term trends under all operating states.

tures.

Table 5: Performance evaluation and comparison results based on different methods.

Feature extractor	Classifier	Accuracy (%)
PCA	SVM	89.5
DPCA		93.9
DLDA		96.5
MFE		98.7
PCA	BLS	91.2
DPCA		92.6
DLDA		84.3
MFE		98.9

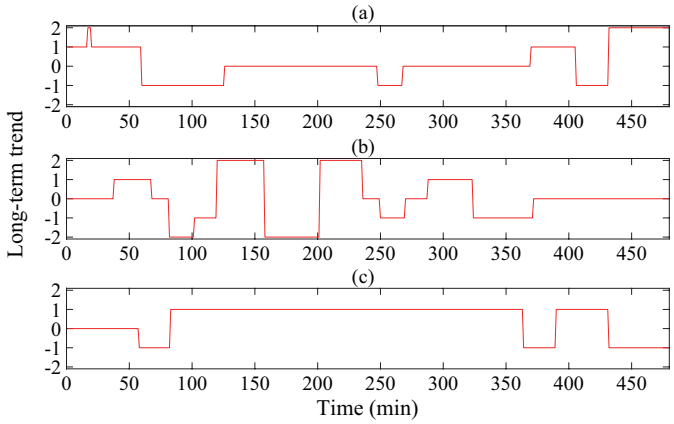

Figure 9: Long-term trends of of the separator water temperature under (a) the normal state, (b) fault 1, and (c) fault 2, respectively.

5.2. Fault Diagnosis Results and Comparisons

Given the above extracted features obtained using the MFE method, this subsection investigates the performance of the fault diagnosis subsystem corresponding to different combinations of features, evaluates the overall performance of the proposed method, and presents comparison results with the state-of-the-art methods.

Figs. 10 and 11 show the fault diagnosis results corresponding to different feature combinations listed in Table 2. The horizontal axis presents the feature combination tags, namely, $C_1, C_2, \cdots, C_{15}$, and the vertical axis denotes the fault diagnosis accuracy. Fig. 11 shows the fault diagnosis results of different feature combinations, where the other three evaluation indicators are considered. It can be found that the feature combinations C_5, C_{10}, C_{11}, C_{12}, C_{13}, and C_{15} led to much higher accuracies compared to other feature combinations, and thus the 6 feature combinations were exploited in the designed subsystems. Table 6 shows the feature combination parameters of the offline rule base, including the selected feature combinations, the number of layers of fault diagnosis sub-system, and the calculated weight parameters. For instance, C_{15} results in a higher accuracy compared to the other combinations, and thus a higher weight is assigned to C_{15}.

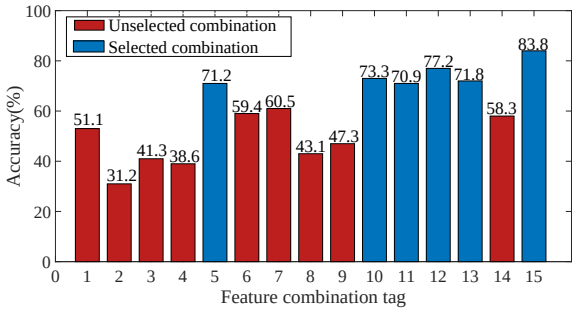

Figure 10: Fault diagnosis accuracy under different feature combinations.

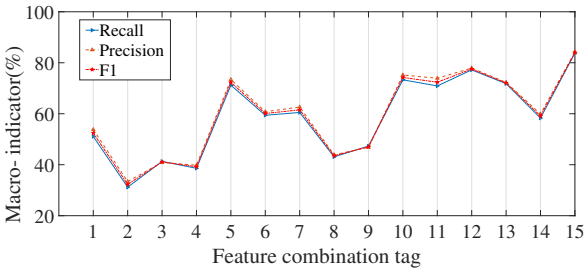

Figure 11: Fault diagnosis results of different feature combinations.

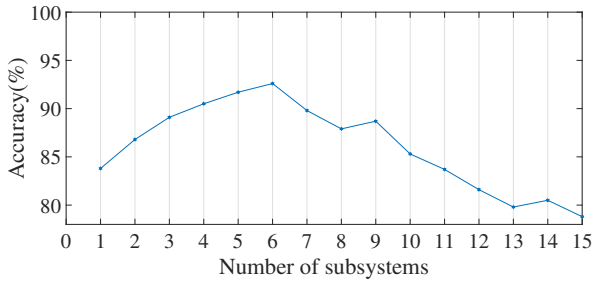

Figure 12: Performance of fault diagnosis subsystem fusion

Table 6: Feature combination parameters of the offline rule base.

Combination	Layers	Accuracy (%)	Weight (%)
C_5	11	71.2	15.9
C_{10}	9	73.3	16.4
C_{11}	7	70.9	15.8
C_{12}	8	77.2	17.2
C_{13}	6	71.8	16.0
C_{15}	5	83.8	18.7

With the above selected six feature combinations, the decision-weighted fusion results are obtained and shown in Fig. 13. It can be seen that the overall accuracy of the proposed method after decision fusion was much higher than that of each single fault diagnosis sub-system with one feature combination. The result of the decision weighted fusion method reached 92.6%, which was increased by 8.8% compared to the highest accuracy of 83.8% without fusion. The above results prove that the constructed fault diagnosis structure and the decision-weighted fusion strategy can effectively improve the fault diagnosis performance.

Fig. 14 shows the confusion matrix of fault diagnosis results of the proposed method. The rows of the matrix represent the actual labels, the columns represent the predicted labels, and the diagonal elements correspond to the classification performance for each category. The fault diagnosis performance was evaluated in terms of the accuracy. Most diagonal elements were over 0.90 except for fault

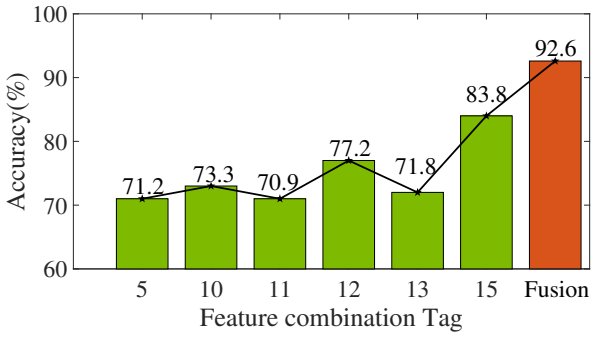

Figure 13: Decision weighted fusion results.

3 (0.73), fault 9 (0.73), fault 15 (0.69), and the normal state (0.81). In the presence of faults 3, 9, and 15, the trend changes of the process signals were not significant, which made it relatively more challenging to identify such fault types accurately.

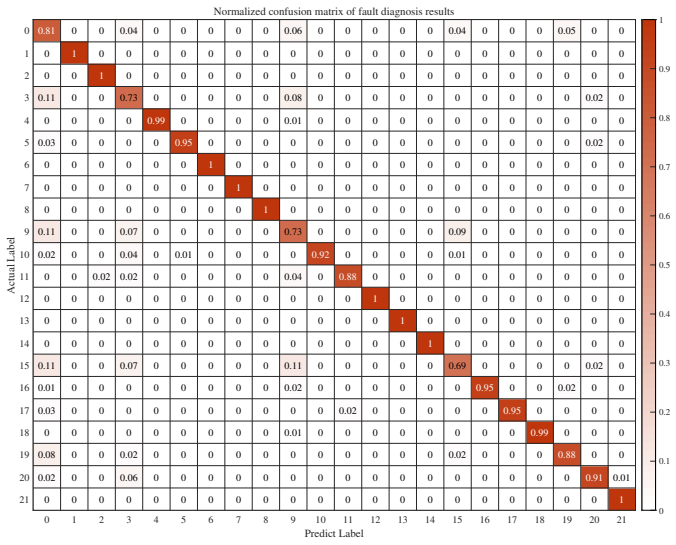

Figure 14: Confusion matrix using the proposed fault diagnosis method.

To demonstrate the superiority of the proposed method, Table 7 shows the performance comparison results with two recent deep learning based methods, including the Deep Learning Multi-model Fusion (DLMF) (Wang et al., 2020), the Deep Convolutional Neural Network (DCNN) (Wu and Zhao, 2018), Target Transformer (TT) (Wei et al., 2022), and Improved Long short-term memory Generative adversarial network (ILG) (Du et al., 2023). The performance was evaluated in terms of Precision, Recall, Macro-F1, training time, and test time. The first three indexes of the proposed method, DCNN, and TT exceeded 90% and were higher than those of the DLMF and ILG methods. The precision and macro-F1 score were 93.7% and 93.1%, which were higher than those of DCNN and TT. Moreover, the proposed was much computationally faster than DCNN, TT and ILG methods as demonstrated by the training and test time. Such an advantage is owing to the flat struc-

ture of the BLS, while in DCNN, a deep structure leads to a larger number of parameters and more complex computation to reach high performance. More detailed results for all different operating states using the three methods are given in Table 8. It is obvious that the proposed method showed better fault diagnosis performance compared to those of the other four deep learning models in most states. Hence, the proposed method performed well in fault diagnosis and met the requirements of online diagnosis and model updating. This also demonstrates the adaptability of the method for multiple classes of faults.

Since fault diagnosis is a dynamic process, exploring the diagnostic performance in the presence of unknown faults is necessary. A comparison test was designed to include unknown faults. In this experiment, the system was in a normal state in the first 3 hours, and then an unknown fault was injected in during the period from the 3rd hour to the 4th hour. The system returned to normal after the 4th hour. Table 9 provides a comparison of results using the five methods in simulating online fault diagnosis. In the first 3 hours, the accuracy of all methods was over 85% except for TT, showing good performance. In the period of 3-4 h under the unknown fault condition, the proposed method showed higher accuracy than the other four methods. This proves that the proposed method is more effective in detecting unknown faults than other methods. The results also prove the good adaptability of the proposed method to unknown faults.

6. Conclusion

This study proposed a new data-driven fault diagnosis method based on the multi-feature fusion and weighted timeliness Broad Learning System (BLS). First, the fault-related multi-features, including short-term trends, long-term trends, and binary alarm signals, were extracted from the original process data. Then, a fault diagnosis model was established by importing the multi-features into the modified BLS, where weighted parameters were designed to balance the timeliness and accuracy of the diagnostic subsystem. The effectiveness and superiority of the proposed method were demonstrated based on the benchmark Tennessee Eastman (TE) process. According to the results, the proposed method obtained fault-related features effectively, and outperformed the existing approaches for online and unknown fault diagnosis. The effective identification of multiple faults and the detection of unknown faults demonstrate the adaptability of the proposed method. In conclusion, the proposed method provides an effective dynamic online fault diagnosis method for complex industrial processes by capturing multiple features and establishing the BLS based diagnostic model.

The proposed method can be applied to fault diagnosis in petroleum, chemical, and metallurgical processes. By embedding the diagnosis algorithm into industrial personal computers or distributed control systems, the online fault diagnosis results can alert operators to deal with faults as early as possible to avoid accidents. A future direction will be concentrated on improving the sensitivity of the fault diagnosis algorithm to unknown faults. A potential solution would be to introduce transfer learning methods to learn faulty features from other similar processes.

Declaration of competing interest

The authors declare that they have no known competing financial interests or personal relationships that could have appeared to influence the work reported in this paper.

Acknowledgments

This work was supported by the Key Program of Hubei Provincial Technical Innovation Project under Grant No. 2023BAB080, in part by the Knowledge Innovation Program of Wuhan-Shuguang Project under Grant No. 2022010801020208, and in part by the CUG Scholar Scientific Research Funds at China University of Geosciences (Wuhan) under Grant 2023071.

Reference

Abdi, H., et al., 2007. The method of least squares. Encyclopedia of measurement and statistics 1, 530–532.

Amin, M.T., Khan, F., Ahmed, S., Imtiaz, S., 2021. A data-driven bayesian network learning method for process fault diagnosis. Process Safety and Environmental Protection 150, 110–122.

Arunthavanathan, R., Khan, F., Ahmed, S., Imtiaz, S., 2021. A deep learning model for process fault prognosis. Process Safety and Environmental Protection 154, 467–479.

Bai, Y., Zhao, J., 2023. A novel transformer-based multi-variable multi-step prediction method for chemical process fault prognosis. Process Safety and Environmental Protection 169, 937–947.

Cai, B., Fan, H., Shao, X., Liu, Y., Liu, G., Liu, Z., Ji, R., 2021. Remaining useful life re-prediction methodology based on wiener process: Subsea christmas tree system as a case study. Computers & Industrial Engineering 151, 106983.

Cai, B., Shao, X., Liu, Y., Kong, X., Wang, H., Xu, H., Ge, W., 2020. Remaining useful life estimation of structure systems under the influence of multiple causes: Subsea pipelines as a case study. IEEE Transactions on Industrial Electronics 67, 5737–5747.

Cao, L., Yu, F., Yang, F., Cao, Y., Gopaluni, R.B., 2020. Data-driven dynamic inferential sensors based on causality analysis. Control Engineering Practice 104, 104626.

Chen, C.P., Liu, Z., 2018. Broad learning system: An effective and efficient incremental learning system without the need for deep architecture. IEEE Transactions on Neural Networks and Learning Systems 29, 10–24.

Chen, S., Yang, R., Zhong, M., 2021. Graph-based semi-supervised random forest for rotating machinery gearbox fault diagnosis. Control Engineering Practice 117, 104952.

Chen, X., Zhao, C., 2021. Linear and nonlinear hierarchical multivariate time delay analytics for dynamic modeling and process monitoring. Journal of Process Control 107, 83–93.

Cheng, H., Liu, Y., Huang, D., Cai, B., Wang, Q., 2021. Rebooting kernel CCA method for nonlinear quality-relevant fault detection in process industries. Process Safety and Environmental Protection 149, 619–630.

Cheng, Y., Zhu, H., Wu, J., Shao, X., 2019. Machine health monitoring using adaptive kernel spectral clustering and deep long short-term memory recurrent neural networks. IEEE Transactions on Industrial Informatics 15, 987–997.

Table 7: Comparison results for fault diagnosis based on different methods.

Method	Precision (%)	Recall (%)	Macro-F1 (%)	Training time(s)	Test time(ms)
Proposed method	93.7	92.6	93.1	8.8	0.12
DLMF	89.4	89.3	89.4	793.1	3.5
DCNN	91.3	90.9	91.2	24.3	1.5
TT	90.4	91.2	90.8	420.0	18.0
ILG	90.8	89.6	90.2	220	95

Table 8: Comparison results for fault diagnosis using different methods in terms of F1 score (%).

State	Proposed method	DLMF	DCNN	TT	ILG
Normal	69.5	63.3	79.1	70.3	72.5
1	100.0	99.8	100.0	99.8	99.2
2	99.0	99.8	98.5	98.4	100.0
3	71.2	65.6	60.6	52.7	65.7
4	99.5	95.1	99.3	99.6	98.2
5	96.9	95.6	98.6	91.9	99.1
6	100.0	100.0	99.6	98.2	100.0
7	100.0	100.0	97.6	100.0	99.2
8	100.0	99.0	98.0	95.6	95.2
9	70.9	72.7	62.2	68.7	58.5
10	95.8	92.6	98.2	97.1	98.4
11	92.6	88.3	97.6	98.1	98.28
12	100.0	98.0	99.2	97.1	100.0
13	100.0	98.2	99.8	96.1	100.0
14	100.0	96.3	98.2	98.8	100.0
15	74.6	67.2	42.6	34.1	43.7
16	97.4	89.7	95.8	99.4	97.7
17	97.4	92.7	94.1	94.8	100.0
18	99.6	96.7	98.2	94.6	93.3
19	90.2	85.2	99.2	98.7	87.6
20	92.4	87.6	92.8	94.3	100.0
21	100.0	82.5	97.2	98.6	89.3

Table 9: Comparison results for detecting unknown faults of different methods (%).

Time period	0-1h	1-2h	2-3h	3-4h(Unknown fault)	4-5h	5-6h	6-7h
Proposed metohd	88.6	90.8	89.9	78.9	89.4	89.4	88.5
DCNN	85.1	87.7	87.9	56.8	86.3	86.6	88.1
DLMF	89.3	89.4	88.6	68.8	87.8	86.9	87.2
TT	72.7	88.4	91.2	55.9	88.5	89.3	90.5
ILG	87.5	88.8	88.5	74.5	87.8	88.2	88.4

Dong, Y., Qin, S.J., 2018. A novel dynamic PCA algorithm for dynamic data modeling and process monitoring. Journal of Process Control 67, 1–11.

Du, W., Yang, J., Meng, G., 2023. Fault diagnosis for dynamic system based on the independent latent space reconstruction of generative adversarial network. Journal of Process Control 125, 28–40.

Fu, Y., Cao, H., Chen, X., Ding, J., 2023. Improved broad learning system for machinery intelligent fault diagnosis with increasing fault samples, fault modes, and running conditions. ISA transactions 136, 400–416.

Gao, Z., Dang, W., Liu, M., Guo, W., Ma, K., Chen, G., 2021. Classification of EEG signals on VEP-based BCI systems with broad learning. IEEE Transactions on Systems, Man, and Cybernetics: Systems 51, 7143–7151.

Hoang, D.T., Kang, H.J., 2019. Rolling element bearing fault diagnosis using convolutional neural network and vibration image. Cognitive Systems Research 53, 42–50.

Hu, W., Wang, J., Yang, F., Han, B., Wang, Z., 2022. Analysis of time-varying cause-effect relations based on qualitative trends

and change amplitudes. Computers & Chemical Engineering 162, 107813.
Ji, H., He, X., Shang, J., Zhou, D., 2017. Incipient fault detection with smoothing techniques in statistical process monitoring. Control Engineering Practice 62, 11–21.
Kong, X., Cai, B., Liu, Y., Zhu, H., Liu, Y., Shao, H., Yang, C., Li, H., Mo, T., 2022. Optimal sensor placement methodology of hydraulic control system for fault diagnosis. Mechanical Systems and Signal Processing 174, 109069.
Li, Q., Ding, X., He, Q., Huang, W., Shao, Y., 2021a. Manifold sensing-based convolution sparse self-learning for defective bearing morphological feature extraction. IEEE Transactions on Industrial Informatics 17, 3069–3078.
Li, X., Guo, M., Chen, G., 2023a. A hybrid algorithm for inspection planning of subsea pipelines subject to corrosion-fatigue degradation. Process Safety and Environmental Protection 178, 685–694.
Li, X., Ma, J., Pasman, H., Zhang, R., 2023b. Dynamic risk investigation of urban natural gas pipeline accidents using stochastic petri net approach. Process Safety and Environmental Protection 178, 933–946.
Li, Y., Cao, W., Hu, W., Wu, M., 2020. Diagnosis of downhole incidents for geological drilling processes using multi-time scale feature extraction and probabilistic neural networks. Process Safety and Environmental Protection 137, 106–115.
Li, Y., Cao, W., Hu, W., Wu, M., 2023c. Identification of downhole conditions in geological drilling processes based on quantitative trends and expert rules. Neural Computing and Applications 35, 12297–12306.
Li, Y., Wang, S., Li, N., Deng, Z., 2021b. Multiscale symbolic diversity entropy: a novel measurement approach for time-series analysis and its application in fault diagnosis of planetary gearboxes. IEEE Transactions on Industrial Informatics 18, 1121–1131.
Liu, K., Cai, B., Wu, Q., Chen, M., Yang, C., Khan, J.A., Wang, C., Pattiyakumbura, H.V.W., Ge, W., Liu, Y., 2023. Risk identification and assessment methods of offshore platform equipment and operations. Process Safety and Environmental Protection 177, 1415–1430.
Liu, Q., Song, B., Ding, X., Qin, S.J., 2022a. Fault diagnosis of dynamic processes with reconstruction and magnitude profile estimation for an industrial application. Control Engineering Practice 121, 105008.
Liu, Q., Wang, Z., He, X., Zhou, D., 2018. Event-triggered resilient filtering with measurement quantization and random sensor failures: Monotonicity and convergence. Automatica 94, 458–464.
Liu, Y., Wang, Z., Zou, L., Zhou, D., Chen, W.H., 2022b. Joint state and fault estimation of complex networks under measurement saturations and stochastic nonlinearities. IEEE Transactions on Signal and Information Processing over Networks 8, 173–186.
Lu, Q., Yang, R., Zhong, M., Wang, Y., 2020. An improved fault diagnosis method of rotating machinery using sensitive features and RLS-BP neural network. IEEE Transactions on Instrumentation and Measurement 69, 1585–1593.
Lucke, M., Chioua, M., Grimholt, C., Hollender, M., Thornhill, N.F., 2020a. Integration of alarm design in fault detection and diagnosis through alarm-range normalization. Control Engineering Practice 98, 104388.
Lucke, M., Stief, A., Chioua, M., Ottewill, J.R., Thornhill, N.F., 2020b. Fault detection and identification combining process measurements and statistical alarms. Control Engineering Practice 94, 104195.
Men, J., Chen, G., Reniers, G., Rao, X., Zeng, T., 2023. A hybrid deep belief network-based label distribution learning system for seismic damage estimation of liquid storage tanks. Process Safety and Environmental Protection 172, 908–922.
Pan, Q., Zhang, L., Dai, G., Zhang, H., 1999. Two denoising methods by wavelet transform. IEEE Transactions on Signal Processing 47, 3401–3406.
Pu, X., Li, C., 2021. Online semisupervised broad learning system for industrial fault diagnosis. IEEE Transactions on Industrial Informatics 17, 6644–6654.
Ricker, N.L., 1996. Decentralized control of the tennessee eastman challenge process. Journal of process control 6, 205–221.
Shang, J., Chen, M., Zhang, H., Ji, H., Zhou, D., Zhang, H., Li, M., 2018. Increment-based recursive transformed component statistical analysis for monitoring blast furnace iron-making processes: An index-switching scheme. Control Engineering Practice 77, 190–200.
Song, B., Yan, H., Shi, H., Tan, S., 2020. Multisubspace elastic network for multimode quality-related process monitoring. IEEE Transactions on Industrial Informatics 16, 5874–5883.
Song, J., He, X., 2023. Robust state estimation and fault detection for autonomous underwater vehicles considering hydrodynamic effects. Control Engineering Practice 135, 105497.
Uddin, Z., Qamar, A., Alam, F., 2021. ICA based sensors fault diagnosis: an audio separation application. Wireless Personal Communications 118, 3369–3384.
Vairo, T., Cademartori, D., Clematis, D., Carpanese, M.P., Fabiano, B., 2023. Solid oxide fuel cells for shipping: A machine learning model for early detection of hazardous system deviations. Process Safety and Environmental Protection 172, 184–194.
Wang, J., Yu, Y., Chen, K., 2019. Determining the number of segments for piece-wise linear representation of discrete-time signals. Computers & Chemical Engineering 120, 46–53.
Wang, N., Yang, F., Zhang, R., Gao, F., 2020. Intelligent fault diagnosis for chemical processes using deep learning multimodel fusion. IEEE Transactions on Cybernetics 52, 7121–7135.
Węglarczyk, S., 2018. Kernel density estimation and its application, in: ITM Web of Conferences, EDP Sciences. p. 00037.
Wei, Z., Ji, X., Zhou, L., Dang, Y., Dai, Y., 2022. A novel deep learning model based on target transformer for fault diagnosis of chemical process. Process Safety and Environmental Protection 167, 480–492.
Wu, H., Zhao, J., 2018. Deep convolutional neural network model based chemical process fault diagnosis. Computers & chemical engineering 115, 185–197.
Xie, T., Huang, X., Choi, S.K., 2022. Intelligent mechanical fault diagnosis using multisensor fusion and convolution neural network. IEEE Transactions on Industrial Informatics 18, 3213–3223.
Yang, G., Gu, X., 2019. Fault diagnosis of complex chemical processes based on enhanced naive bayesian method. IEEE Transactions on Instrumentation and Measurement 69, 4649–4658.
Yang, L., Yang, Z., Song, S., Li, F., Chen, C.L.P., 2023. Twin broad learning system for fault diagnosis of rotating machinery. IEEE Transactions on Instrumentation and Measurement 72, 1–12.
Yin, S., Zhu, X., Kaynak, O., 2015. Improved PLS focused on key-performance-indicator-related fault diagnosis. IEEE Transactions on Industrial Electronics 62, 1651–1658.
Yu, W., Zhao, C., 2020. Broad convolutional neural network based industrial process fault diagnosis with incremental learning capability. IEEE Transactions on Industrial Electronics 67, 5081–5091.
Zhang, J., Cai, B., Mulenga, K., Liu, Y., Xie, M., 2018. Bayesian network-based risk analysis methodology: A case of atmospheric and vacuum distillation unit. Process Safety and Environmental Protection 117, 660–674.
Zhang, X., Du, M., Wang, Y., Zhang, H., Guo, Y., 2023. Research on power grid fault diagnosis based on a quantitative representation of alarm information. IEEE Transactions on Industrial Electronics 70, 9582–9592.